Corrosion Science 223 (2023) 111470

Contents lists available at ScienceDirect

Corrosion Science

journal homepage: www.elsevier.com/locate/corsci

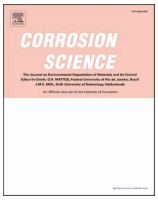

Laser ablation behavior of a 2-D C/SiC-Ti_3SiC_2 composite

Te Ma [a,b], Hongwei Song [a,b,*], Cheng Qiu [a], Wu Yuan [a,b], Ruixing Wang [a]

[a] Key Laboratory for Mechanics in Fluid Solid Coupling Systems, Institute of Mechanics, Chinese Academy of Sciences, Beijing 100190, China
[b] School of Engineering Science, University of Chinese Academy of Sciences, Beijing 100049, China

ARTICLE INFO

Keywords:
Laser ablation resistance
2-D C/SiC-Ti_3SiC_2 composite
In-situ observation measurement
Decomposition and sublimation
Temperature Jump

ABSTRACT

When subjected to laser irradiation of different power densities, Ti_3SiC_2 MAX phase-modified 2-D C/SiC composite experiences various chemical and physical reactions and demonstrates various ablation resistance. An in-situ observation measurement is developed to obtain the instantaneous mesoscopic ablation process for revealing the ablation mechanism. Then scanning electron microscope (SEM) and X-ray energy dispersive spectroscopy (EDS) tests are performed to determine the reaction process. The results show that the Ti_3SiC_2 MAX phase can effectively prevent laser irradiation into the material at a laser power density below 636.5 W/cm^2. The advantage of ablation resistance disappears at a high laser power density of 2546 W/cm^2 due to the decomposition and sublimation of SiC and Ti_3SiC_2. A chart of ablation mechanisms versus laser power density is constructed based on the instantaneous mesoscopic ablation behavior, macro/meso/microscopic ablation morphology, and temperature history. It is also found that there are two forms of "Temperature Jump" phenomena. One is the accelerated temperature rise in the temperature history of the single-irradiation event. The other is the step point in the maximum temperature curve for multiple irradiation events. The mechanisms of the "Temperature Jump" phenomena are explained based on the interface energy balance.

1. Introduction

As a typical and promising material system, carbon fiber-reinforced silicon carbide ceramic matrix (C/SiC) composites have been increasingly applied to thermal protection systems (TPS) of high-performance vehicles such as hypersonic aircraft [1–3]. Although C/SiC composites have quite a few characteristics, such as high fracture toughness, good ablation resistance, and sound mechanical performance [4–10], it is difficult to serve at the temperature above 2000 K for an extended period due to the active oxidation of the SiC matrix. Therefore, not only carbides, nitrides, and borides have been introduced as ultra-high temperature ceramics (UHTCs), but also MAX phases-modified C/SiC composites have been developed to improve the ablation resistance [11–15].

Ti_3SiC_2, as a comprehensive MAX phases ceramic, has good oxidation resistance and high strength performance at the high temperature. It also has similar physical properties to metals, such as thermal conductivity, machinability, and plasticity. Therefore, the Ti_3SiC_2 MAX phase is introduced into C/SiC composites to improve mechanical properties and ablation resistance. As for the ablation performance of C/SiC-Ti_3SiC_2 composites, previous studies have mainly investigated the ablation resistance under oxyacetylene flame conditions. Fan et al. [16] showed that the mass and linear ablation rates of the C/SiC-Ti_3SiC_2 composite prepared by two-dimensional prefabrication with laminated carbon cloth were significantly lower than those of C/SiC and C/SiC-Si after 20 s exposure to an oxyacetylene flame, implying that the ablation resistance was significantly improved. Yaghobizadeh et al. [17] found that Ti_3SiC_2 modified C_f-C-SiC composite exhibited good ablation resistance when ablated with an oxyacetylene flame ablation. The primary mechanism for ablation resistance was attributed to the stability of the oxide layer in the MAX-containing composite. However, the heat flux and ablation temperature of oxyacetylene flame examination are limited by the maximum flame temperature (about 3270 K). The combustion products (including O_2, CO_2, O, OH and H_2O) lead to a deviation from the actual gas concentration and a deviation from the actual ablation performance of the materials [18].

Recently, the high-power laser has been employed to perform ablation tests. The high-power laser, with its characteristics of high spectral purity, spatial and temporal coherence, and high intensity [19–21], can also be used as a stable and controllable heat source with an adjustable

* Corresponding author at: Key Laboratory for Mechanics in Fluid Solid Coupling Systems, Institute of Mechanics, Chinese Academy of Sciences, Beijing 100190, China.
E-mail address: songhw@imech.ac.cn (H. Song).

https://doi.org/10.1016/j.corsci.2023.111470
Received 17 January 2023; Received in revised form 22 August 2023; Accepted 23 August 2023
Available online 25 August 2023
0010-938X/

heat flux from very low to extremely high. Tests with laser irradiation have been successful in researching the ablation performance of composite materials, and the ambient atmosphere can be customized according to the actual conditions [22–31]. However, to date, few studies have been on the laser ablation resistance of C/SiC composites, especially MAX phase-modified C/SiC composites. Tong et al. [32,33] investigated the ablation resistance of C/SiC composites with the pulsed laser and analyzed the ablation mechanisms based on the morphology of different areas after laser ablation. Wang et al. [34] investigated the ablation behavior of 2-D C/SiC composites with a continuous wave laser in tangential supersonic airflow and static air environments. The microstructure of the ablation zone was measured. The effects of supersonic airflow on the ablation morphology and ablation rate of C/SiC composites were analyzed. Pan et al. [35] reported the effects of laser parameters on the ablation mechanisms of the C/SiC composite. The results showed that both power density and pulse number significantly affect on surface morphology and ablation behavior. Wang et al. [36,37] reported a unique "avalanche" phenomenon in the laser irradiation experiments on C/SiC composites in a hypersonic wind tunnel, the ablation rate under tangential hypersonic airflow is significantly higher than that in the static air environment. The coupled thermal-fluid-ablation numerical analysis revealed that the additional erosion and accelerated sublimation are the primary mechanisms for the "avalanche". Nevertheless, systematic research on the laser ablation behavior and mechanism of MAX phase-modified C/SiC composites needs to be completed.

This work aims to investigate the ablation resistance of the 2-D C/SiC-Ti_3SiC_2 composite through the laser ablation method. The effect of laser power density on the ablation behavior is systematically studied. In-situ observation measurement is established to determine the instantaneous laser ablation behavior at the meso-scale. Laser ablation mechanisms are explained in terms of the instantaneous mesoscopic ablation behavior, macro/meso/microscopic ablation morphology, and temperature responses. The mechanisms of the "Temperature Jump" phenomena in the temperature curves are explained. The ablation data of 2-D C/SiC composites with or without T_3SiC_2 are compared, and the reasons for the difference are analyzed. The MAX phase-modified C/SiC composite can undergo different chemical and physical reactions and exhibit different ablation resistance upon laser irradiation with different power densities. The study is helpful to reveal the ablation mechanisms of such a modified composite in low to high heat flux environments and thus to evaluate the adaptability of the composite to conditions from a moderate to an extremely high temperature.

2. Experimental setup

2.1. Specimens

In this experiment, 2-D C/SiC and C/SiC-Ti_3SiC_2 specimens are fabricated and provided by the Science and Technology on Thermostructural Composite Materials Laboratory, Northwestern Polytechnical University. The fiber preform is fabricated from T300 carbon fiber (Toray Industries, Japan). Firstly, the pyrolytic carbon (PyC) interface with a thickness of 200 nm is deposited on the fiber preform by chemical vapor infiltration (CVI). Subsequently, the porous C/SiC preforms are prepared by depositing the SiC matrix by the CVI method. Argon is chosen as the diluent gas during the fabrication to control the reaction rate. High-purity H_2 is used as a carrier gas for MTS, and MTS is introduced into the reaction chamber by bubbling. Then, the TiC-C particles (60 wt% TiC, 6 wt% C) are introduced into the pores of the porous C/SiC preform by slurry infiltration. The infiltration must be repeated 4 times to ensure the TiC-C particles are introduced into the pores and the C/SiC-TiC-C is obtained. Finally, the samples are put into the vacuum furnace and infiltrated with liquid silicon at 1600 ℃. The processed samples are deposited with the SiC coating. Each substance volume fraction of 2-D C/SiC and 2-D C/SiC-Ti_3SiC_2 composites obtained by the Archimedes drainage method are shown in Table 1. The calculation formulas and the experimental procedure can be seen in Appendix A. The research subject is the modified C/SiC-Ti_3SiC_2 composite and the unmodified C/SiC composite is the control group.

2.2. Experimental procedure

The experimental setup is illustrated in Fig. 1. The instantaneous mesoscopic laser ablation is photographed with the high-speed camera and the continuous zoom microscope lens. The in-situ observation measurement is also used to record the specimen's macro/mesoscopic ablation morphology before and after the experiments. The high-power laser with a wavelength of 1064 nm is used for the experiment. The temperature of the back surface is detected by a platinum-rhodium thermocouple when it is lower than 1870 K, as shown in Fig. 1a. The infrared thermal imager is used for the acquisition of temperature when it is higher than 1870 K, as shown in Fig. 1b. The total laser energy is 4000 J, and the combinations of laser power and total irradiation time are 250 W/16.0 s, 500 W/8.0 s, 750 W/5.3 s, 1000 W/4.0 s and 2000 W/2.0 s, respectively. The diameter of the laser spot is 1.0 cm, and the laser power density (LPD) is 318.3, 636.5, 954.8, 1273 and 2546 W/cm^2, respectively. Each case is performed ten times unless the specimen is burn-through.

3. Results and discussion

3.1. Multiscale ablation behavior

3.1.1. In-situ mesoscopic observation

Fig. 2 shows the instantaneous mesoscopic ablation behavior at an LPD of 318.3 W/cm^2. It can be seen from Fig. 2 that the surface of the specimen is liquid and accompanied by bubbles. Poisson spots are located on the top of the bubbles. It takes 0.75 s from the bubble diameter of 0.42 ± 0.01 mm in Fig. 2a to 0.94 ± 0.01 mm in Fig. 2d, corresponding to an expansion rate of 0.69 ± 0.03 mm/s. Then the phenomena of collapse and merger appear in Fig. 2e and f. Some researchers have studied the bubble phenomenon of silicon carbide during the oxidation process [38–41]. The bubble nucleation and growth are promoted by the high-pressure CO generated in the passive oxidation of silicon carbide. When the bubble formation rate is much higher than the flow rate of silicon dioxide, it may lead to a highly active oxidation rate, thereby reducing the oxidation resistance of silicon carbide [39]. However, since the bubble formation rate is much lower than the fluidity of liquid silica (7 cP), the bubble formation in this paper has little effect on the oxidation resistance. The liquid silica also can heal the local micro-holes formed during the collapse of silica bubbles. As shown in Fig. 2f, the bottom of the transparent silica bubbles is still liquid, indicating that bubbles have formed on the surface of the liquid silica layer. The fibers are not exposed to air even if the bubbles collapse and burst.

Fig. 3 shows the instantaneous ablation behavior when LPD is 636.5 W/cm^2. As seen in the circular red dashed delineations of Fig. 3a to Fig. 3f, a bundle of parallel fibers degenerated to both sides, respectively. Compared to the instantaneous ablation behavior observed at a laser power density of 318 W/cm^2, the exposed condition of the fiber elucidates the occurrence of active oxidation phenomena within both the SiC coating and matrix. When the SiC in the upper layer is dissipated,

Table 1
The each substance volume fraction of 2-D C/SiC and 2-D C/SiC-Ti_3SiC_2 composites.

Composites	Density (g/cm^3)	Porosity (vol%)	Carbon (vol%)	SiC (vol%)	Ti_3SiC_2 (vol%)
2-D C/SiC	2.00	13	54.2	32.8	0
2-D C/SiC -Ti_3SiC_2	2.42	8	54.2	17.5	20.3

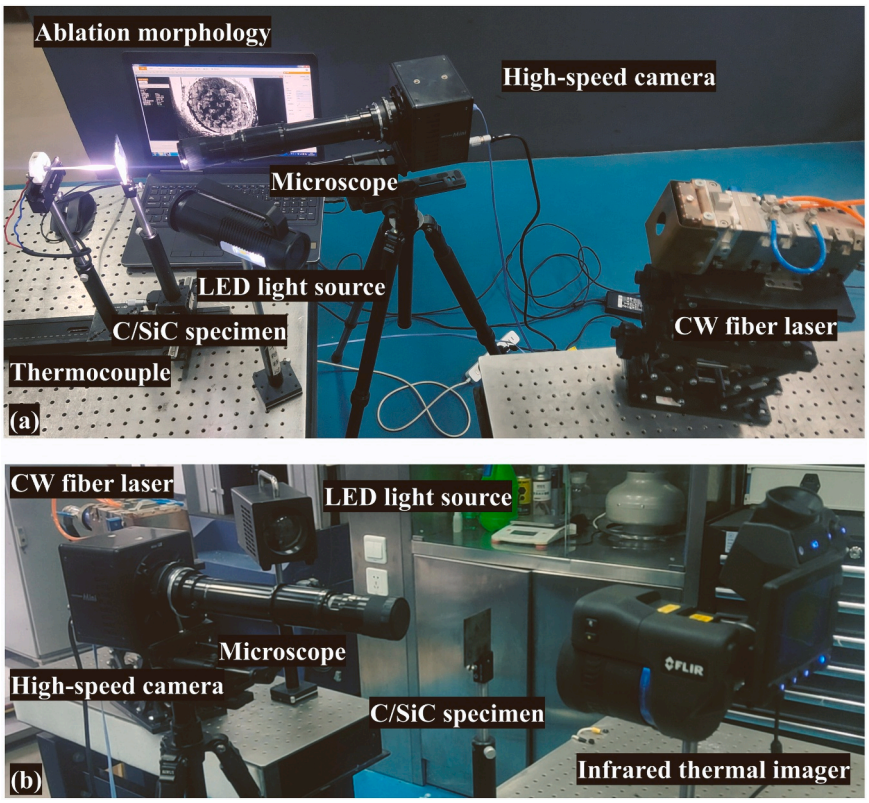

Fig. 1. Photo of experimental installation. (a) The platinum-rhodium thermocouple is adopted when the temperature is lower than 1870 K; (b) the infrared thermal imager is adopted when the temperature is higher than 1870 K.

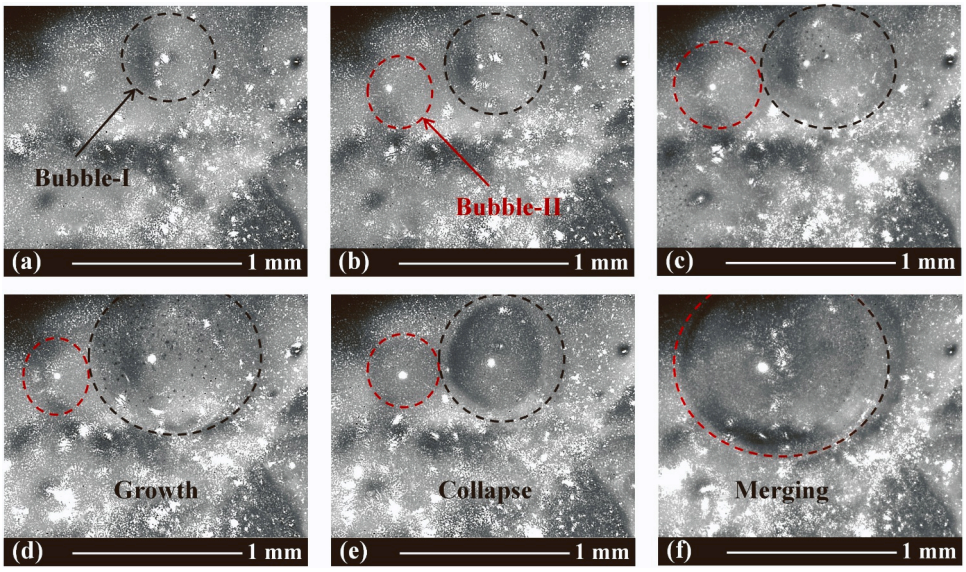

Fig. 2. In-situ observation of bubble evolution during the fifth laser irradiation, when LPD is 318.3 W/cm^2. (a) 6.00 s; (b) 6.25 s; (c) 6.50 s; (d) 6.75 s; (e) 7.00 s; (f) 7.25 s.

the carbon fibers at the top of the fiber bundle are inevitably exposed to air due to the microstructural characteristics of 2-D C/SiC composites. Due to the diameter of the single carbon fiber is about 7 μm, the fibers seen in the image are filamentous. As the duration of laser irradiation increases, the rate of degeneration increases, and the area becomes more extensive. The rippling phenomenon indicates that the liquid oxide, which prevents the oxidation of carbon fibers mainly distributed in the other areas. The liquid oxide may be titanium dioxide formed by the oxidation reaction of the Ti_3SiC_2 MAX phase in the matrix, which can also prevent the oxidation of the carbon fibers.

3.1.2. *Macroscopic/mesoscopic ablation behaviors*

The macroscopic/mesoscopic ablation morphology of the 2-D C/SiC-Ti_3SiC_2 composite at different laser power densities is shown in Fig. 4. Fig. 4a, b, c, d, and e show the ablation morphology at LPD of 318.3, 636.5, 954.8, 1273 and 2546 W/cm^2, respectively. 1, 2, and 3 represent

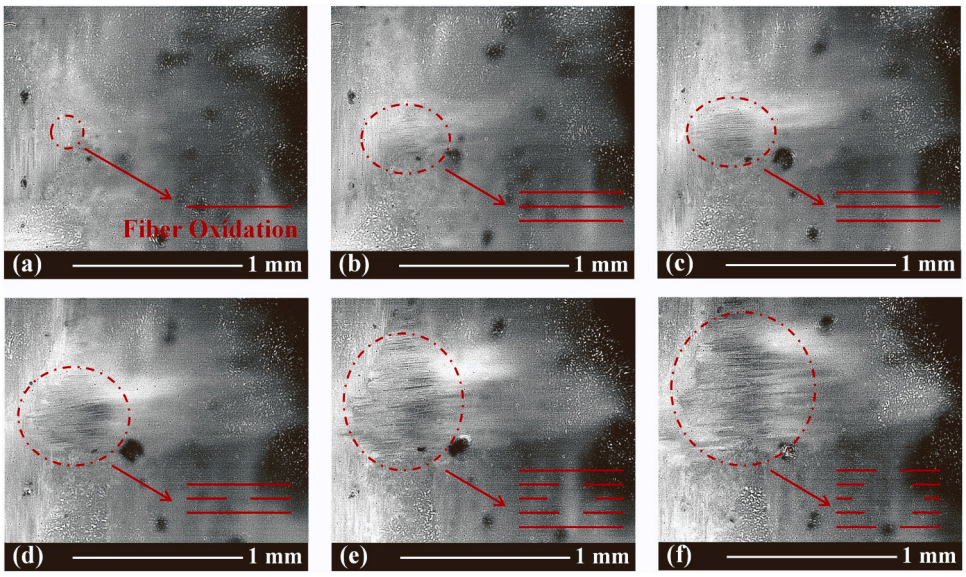

Fig. 3. In-situ observation of fiber bundle oxidation during the fifth laser irradiation, when LPD is 636.5 W/cm^2. (a) 2.75 s; (b) 3.00 s; (c) 3.25 s; (d) 3.50 s; (e) 3.75 s; (f) 4.00 s.

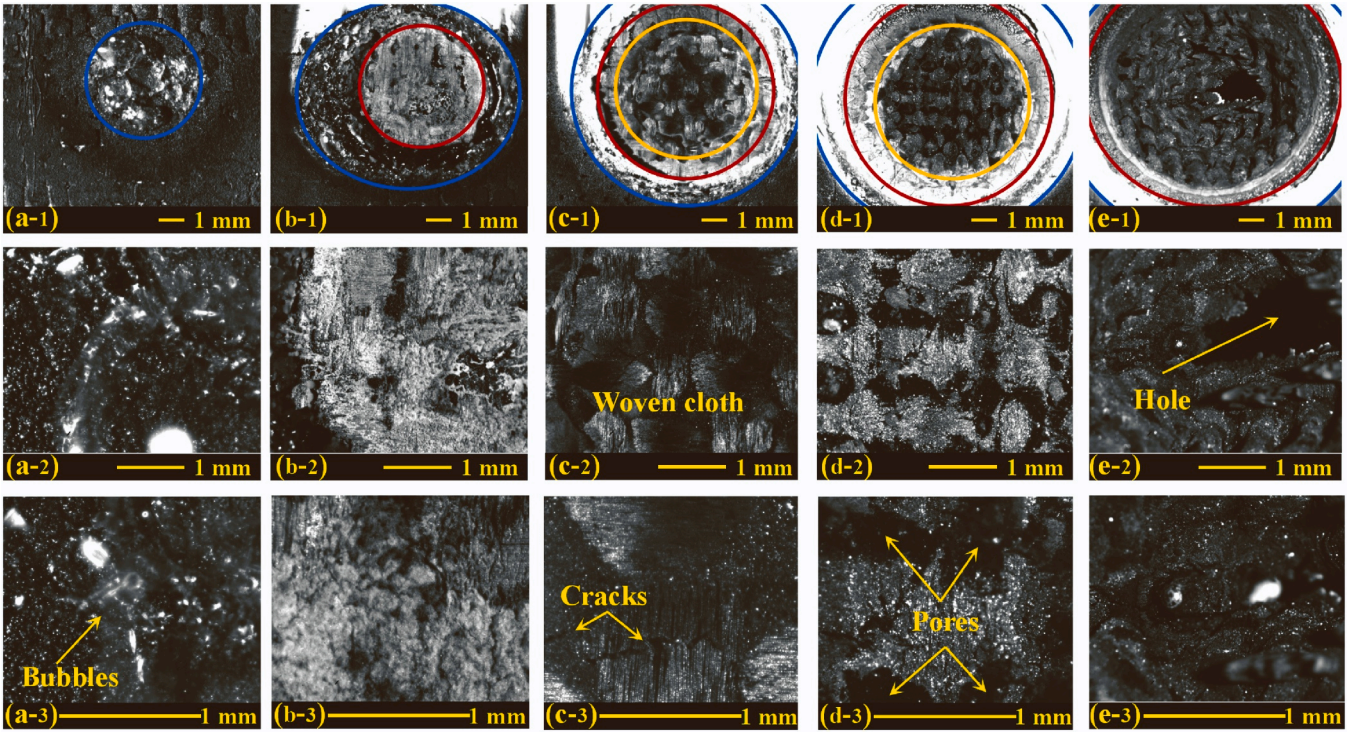

Fig. 4. The laser ablation morphology of 2-D C/SiC-Ti_3SiC_2 composite at different laser power densities. (a) 318.3 W/cm^2; (b) 636.5 W/cm^2; (c) 954.8 W/cm^2; (d) 1273 W/cm^2; (e) 2546 W/cm^2. 1, 2, and 3 represent the ablation morphology at macro-scale, after three times magnification and six times magnification, respectively.

the ablation morphology at macro-scale, after three times magnification and six times magnification, respectively. As shown in Fig.A.1 of Appendix A, the laser ablation morphology of the 2-D C/SiC composite can be generally divided into three specific regions [32], namely the central zone (CZ, the region with the most severe ablation, the red circle area), the transition zone (TZ, the melting or granular ring area around the central zone, the blue circle area) and the edge zone (EZ, the scattered white oxide protective film over and around the ablation zone). However, the 2-D C/SiC-Ti_3SiC_2 composite is different from the 2-D C/SiC composite. When the LPD is 1273 W/cm^2, there is also a white ring-shaped area between the CZ and TZ, which should be the product of the chemical reaction of the Ti_3SiC_2. This area can be called the coverage zone. The size of the ablation region increases with LPD.

Multiple transparent silica bubbles are formed in CZ when LPD is 318.3 W/cm^2. In Figs. 4a-2 and Figs. 4a-3, silica bubbles can be seen, whereas most other positions show granular SiC, and EZ is unformed. In CZ, the braided fibers begin to loom when LPD reaches 636.5 W/cm^2. There are no transparent bubbles or granular silica. Lamellate titanium dioxide is attached to the fiber bundle and the fiber bundle gap, as shown in Figs. 4b-2 and Figs. 4b-3. This phenomenon indicates that the

SiC coating is completely consumed due to active oxidation. It is more obvious for 2-D C/SiC composites, as shown in Fig.A.1b, there is no substance above the woven cloth. The MAX phase begins to take on the role of an antioxidant for 2-D C/SiC-Ti_3SiC_2 composites. TZ presents three states from the inside to the outside. The first is a transparent fused stacked silica product. The second is an ablation morphology of CZ similar to that under the condition of 318.3 W/cm^2, mostly granular oxidation products. Moreover, the third is a black ring. Under this condition, EZ is formed by the scattered white oxide protective film. The size is less than 180° when it is represented by the central radian. When LPD is 954.8 W/cm^2, the diameter of CZ increases to 8.1 mm. The carbon fiber preform at the ablation center is completely exposed to air. There are also cracks due to thermal stress and granular silica in the pores of the 2-D braided structure. Although TZ is still composed of three parts, the width of the molten ring becomes smaller and the area of EZ becomes larger.

The ablation morphology is shown in Fig. 4d when LPD reaches 1273 W/cm^2. The diameter of CZ further increases and the ablation phenomenon becomes more serious. The area of EZ has reached 360°. It can be seen from Figs. 4d-2 and Figs. 4d-3 that the fibers have begun to oxidize seriously, and the closely arranged woven cloth fibers gradually degenerate to form large pores. There are still a tiny number of granular oxidation products in the pores. CZ changes from transparent oxide film to fiber oxidation. TZ changes from a black ring to three rings with smaller ring widths, and EZ changes from 0° to 360° scattering white product. However, this gradual change is broken when LPD is 2546 W/cm^2. 2-D C/SiC-Ti_3SiC_2 composite with a thickness of 2 mm is burn-through after five times laser irradiation, as shown in Figs. 4e-2. Figs. 4e-3 shows ablation area appears to have an evident gradient, resulting in the center of the mesoscopic morphology and the inability to focus on both sides. There are also some particular forms of "hornstone" products in the ablation center. The combination of the scanning electron microscope (SEM) and X-ray energy dispersive spectroscopy (EDS) techniques is further applied to analyze the composition of the "hornstone" product. TZ is no longer an obvious three rings but is completely occupied by EZ.

3.1.3. *Micro-scale ablation morphology*

Figs. 5 to 7 show SEM and EDS results. Fig. 5 gives the micro-scale laser ablation morphology. The SiO_2 bubbles are cleared to clarify the

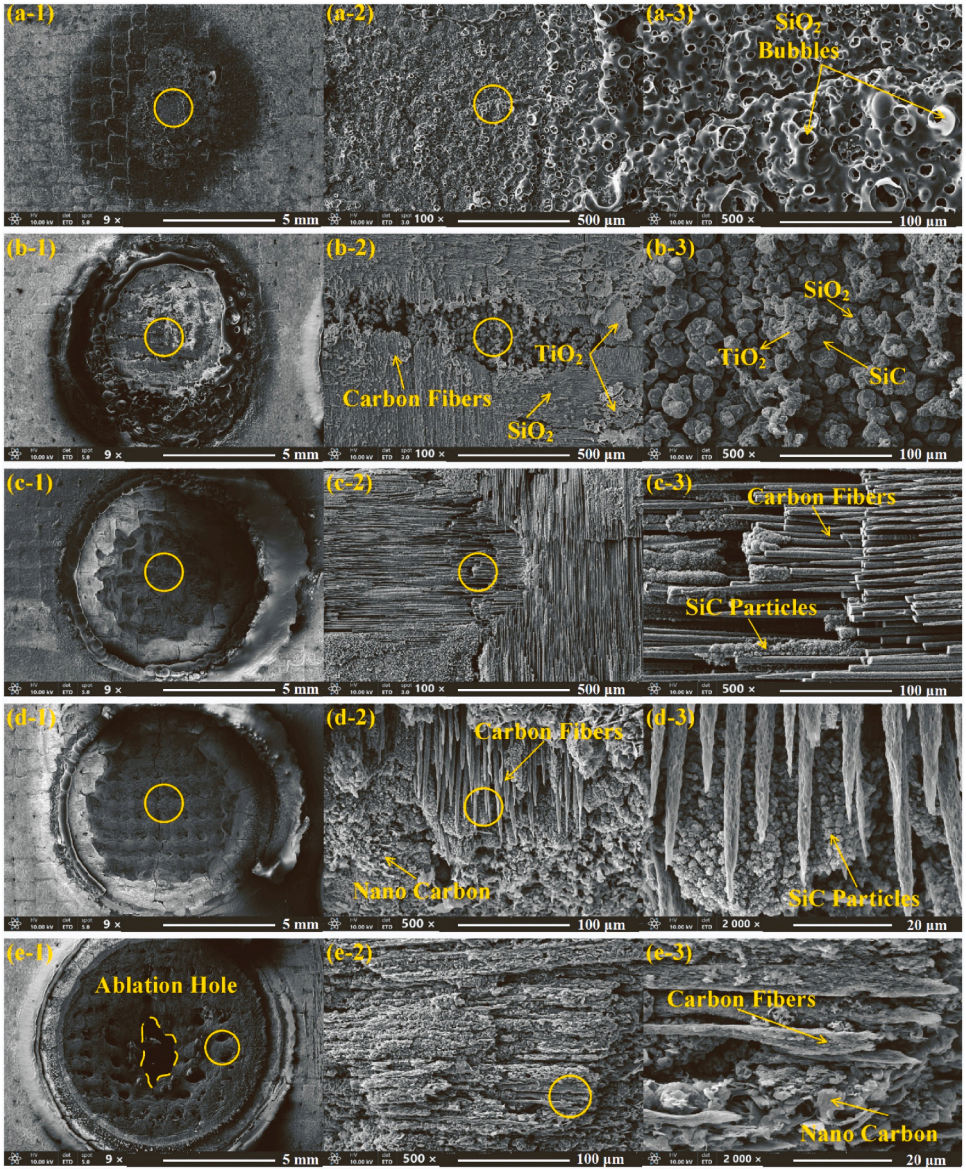

Fig. 5. The microscopic laser ablation morphology of center zone under different laser power densities. (a) 318.3 W/cm^2; (b) 636.5 W/cm^2; (c) 954.8 W/cm^2; (d) 1273 W/cm^2; (e) 2546 W/cm^2. 1, 2, 3 represent the 9, 500 and 2000 times magnification, respectively.

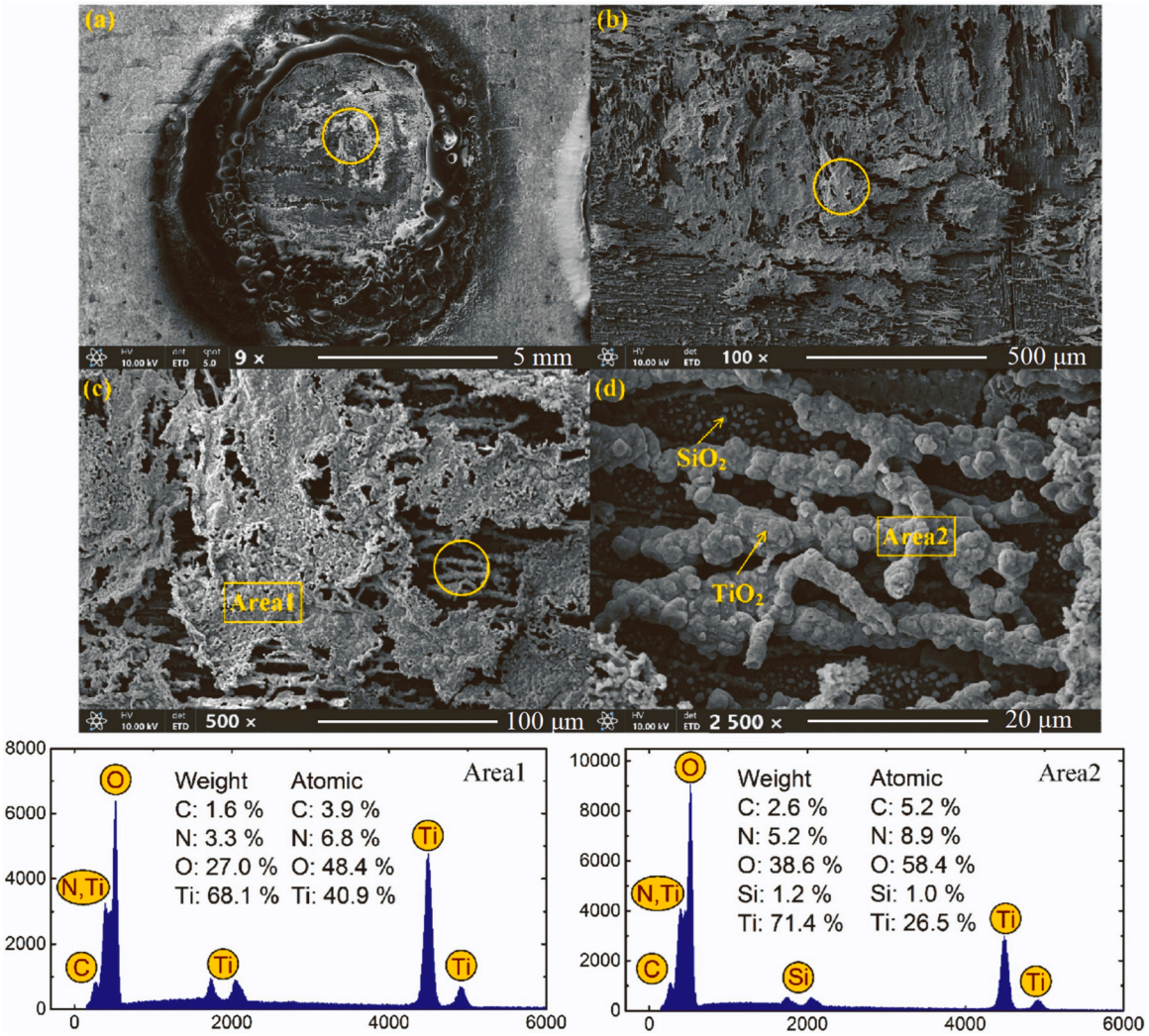

Fig. 6. The microscopic laser ablation morphology of special zone and EDS results when LPD is 636.5 W/cm^2. (a) 9 times magnification; (b) 100 times magnification; (c) 500 times magnification; (d) 2500 times magnification. EDS results of Area1 and Area2 are provided.

lower layer's morphology in Figs. 5a-1. The broken SiO_2 bubbles are on the top of the specimen at the 500 times magnification of the center zone. It can be seen that the center zone includes carbon fibers, spherical SiO_2, and lamellate TiO_2 when LPD is 636.5 W/cm^2. There is granular silicon carbide in the pores of the woven cloth. Those products illustrate the active oxidation of SiC and oxidation of Ti_3SiC_2 matrix are present in the laser ablation process. Furthermore, TiO_2 and SiO_2 melt are insoluble but coexist. SiO_2 melt shrinks into a spherical shape with the rapid cooling of the sample due to the poor wettability between SiO_2 melt and carbon fibers.

Figs. 5c to 5e show that the carbon fibers and fragmented carbon nanoparticles are mainly included in the ablation pit. Carbon nanoparticle content gradually increases with the increase of LPD, and the length of exposed carbon fiber gradually decreases. Meanwhile, carbon fibers have changed from a smooth, spike-like surface to a rough, even irregular state. The mechanism of microscopic ablation morphology of carbon fibers is based on too many parameters [38], such as the reactivity, the volume content of matrix and fiber, the radius of fiber, oxygen concentration, Sherwood number, etc. The above results also show that the microscopic ablation morphology is closely related to the temperature rise rate and temperature caused by different laser power densities.

There are two unusual ablation characteristics in Fig. 6 and Fig. 7.

As shown in Fig. 6, the lamellate TiO_2 widely exists on the top of the laser ablation pit. The large area of lamellate TiO_2 indicates that MAX phase Ti_3SiC_2 generates a large amount of TiO_2 melt, covering the surface of carbon fiber, which can effectively prevent the diffusion of oxygen into the material and improve the anti-oxidation of C/SiC composites. It can be seen from Fig.A.2 of Appendix A that the products of the 2-D C/SiC composite are mainly carbon fibers. And there are only a small amount of SiC particles between the fibers, indicating that the active oxidation rate of SiC is much higher than the oxidation rate of carbon fibers. In Fig. 6d, the morphology of TiO_2 transforms from lamellate to filamentous of 3 μm diameter. Meanwhile, spherical SiO_2 is distributed on the fiber under the filamentous TiO_2. The reason for the formation of filamentous TiO_2 is mainly that TiO_2 melt and SiO_2 melt are produced by the oxidation of Ti_3SiC_2. TiO_2 melt and SiO_2 melt coexist and play the role of anti-oxidation. However, they separate in turning into solid substances and exist on the fiber in different solid forms after laser irradiation. It may be the main reason for the formation of filamentous TiO_2.

As shown in Fig. 7, there are several similar "volcanic" peak-like products with a height of 0.4 mm around the ablation hole at the bottom of the ablation pit. According to the results of EDS analysis, the products near the "crater" and on the volcanic wall are carbon nanoparticles. Therefore, the reason for the formation of products is mainly that the ablation mechanism of the ablation center region is sublimation due to the high temperature when LPD is 2546 W/cm^2. The sublimation rate of the matrix is larger, and the resulting concentration of carbon

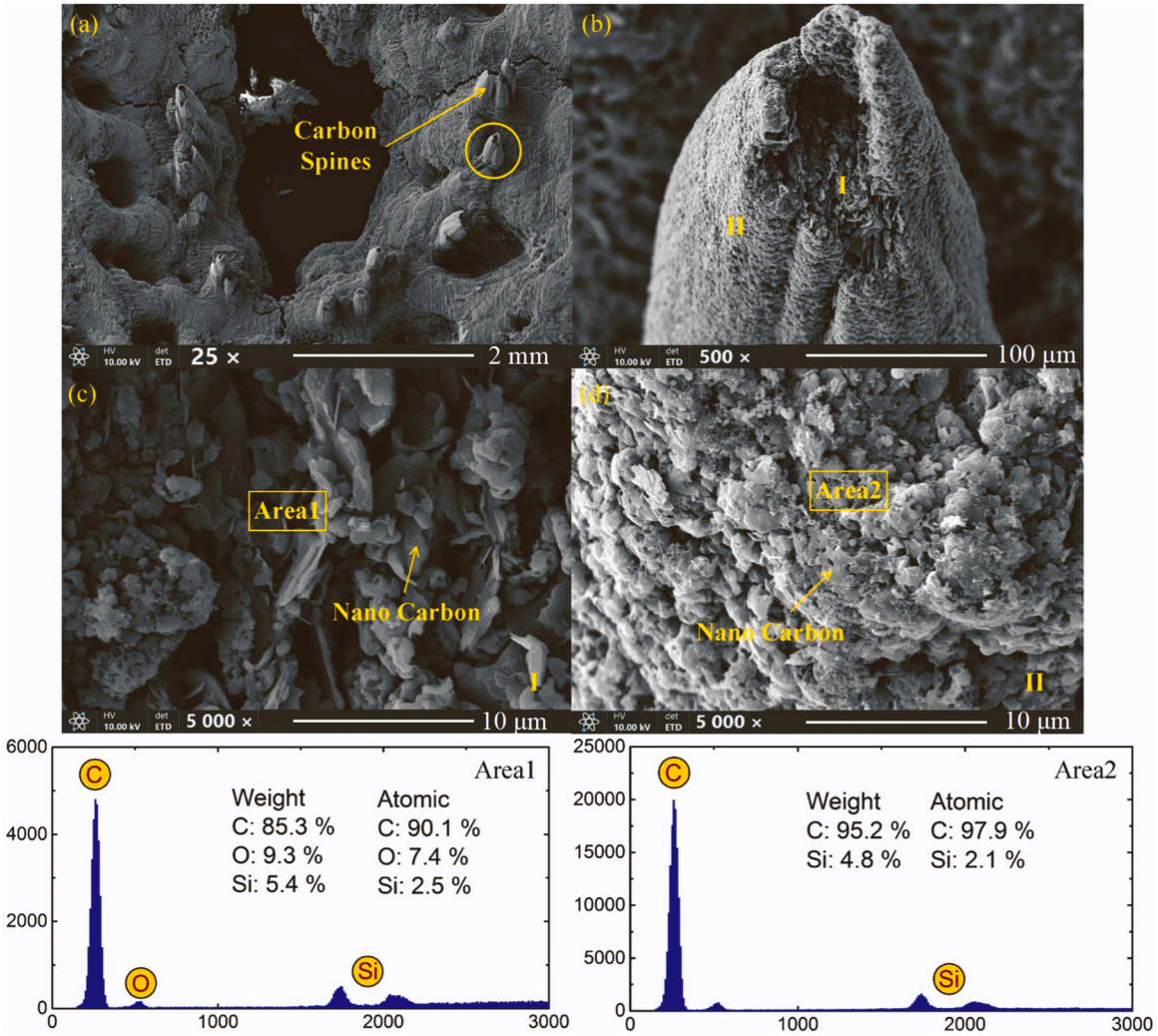

Fig. 7. The microscopic laser ablation morphology of special zone and EDS results when LPD is 2546 W/cm^2. (a) 25 times magnification; (b) 500 times magnification; (c) 5000 times magnification in Area1; (d) 5000 times magnification in Area2. EDS results of Area1 and Area2 are provided.

nanoparticles is also higher. The temperature decreases rapidly due to the convective heat transfer and thermal radiation cooling effect when the laser irradiation is stopped so that a part of the high concentration of carbon nanoparticles urn into a solid state and gradually stack, and finally form a carbon spine.

3.2. Thermal responses

3.2.1. "Temperature jump" phenomena

The temperature curves under different LPD are shown in Fig. 8. According to the curve, the temperature non-linearly rises after each irradiation when LPD is 318.3 W/cm^2. The maximum temperature is 1085 K. Combined with the laser ablation morphology, the SiC coating undergoes passive oxidation. The reaction products in the ablation center zone are mostly granular silica and a small number of transparent silica bubbles. They can play an excellent anti-oxidation effect on carbon fibers. Therefore, C/SiC composites have good reusable performance below the laser power density of 318.3 W/cm^2.

The macroscopic and mesoscopic ablation morphology are given for explaining the potential mechanism of "Temperature Jump" in Fig. 9. Fig. 9a shows that the main characteristics of TZ are still composed of three rings. However, the first ring is a small number of particle products. The area of EZ is less than 180°. CZ, with the most crucial influence on the temperature rise, can be seen as white oxide protective films, cracks and a small amount of granular silica products. Then the phenomenon of "Temperature Jump" appears in the temperature curve. Combined with the white silica powder in the EZ (the white silica produced in this area is mainly due to the unstable silicon monoxide gas generated by silicon carbide in the active oxidation, which overflows to the upper of the laser irradiation and oxidizes into silica), it represents that the silicon carbide in the initial layer has begun to convert from passive to active oxidation during the first laser irradiation. Notwithstanding, the silicon carbide is not completely reactive when the total laser energy is 4000 J. The ablation morphology (as shown in Fig. 9b) and temperature rise curve after the second irradiation are still the same. The maximum temperature is slightly higher than the first irradiation. The white silica powder in EZ increases, and there is still a silica protective film in the central area. In the third irradiation, the temperature curve also shows a "Temperature Jump". Combined with the ablation morphology before and after, the silicon carbide and silicon dioxide on the surface are entirely ablated. The maximum temperature of the unprotected laser irradiation area also increased significantly, and in the fourth and subsequent ablation processes, it is mainly the oxidation of carbon fiber. The "Temperature Jump" phenomenon does not appear again. When LPD increases to 954.8 W/cm^2, the first laser irradiation can completely react with the silicon carbide layer and make a "Temperature Jump" phenomenon appears in the temperature curve. The maximum temperature of the first-time irradiation is slightly lower, about 1523 K. The maximum temperature of the following nine times is about 1573 K. The same is true for a thermal response when LPD is

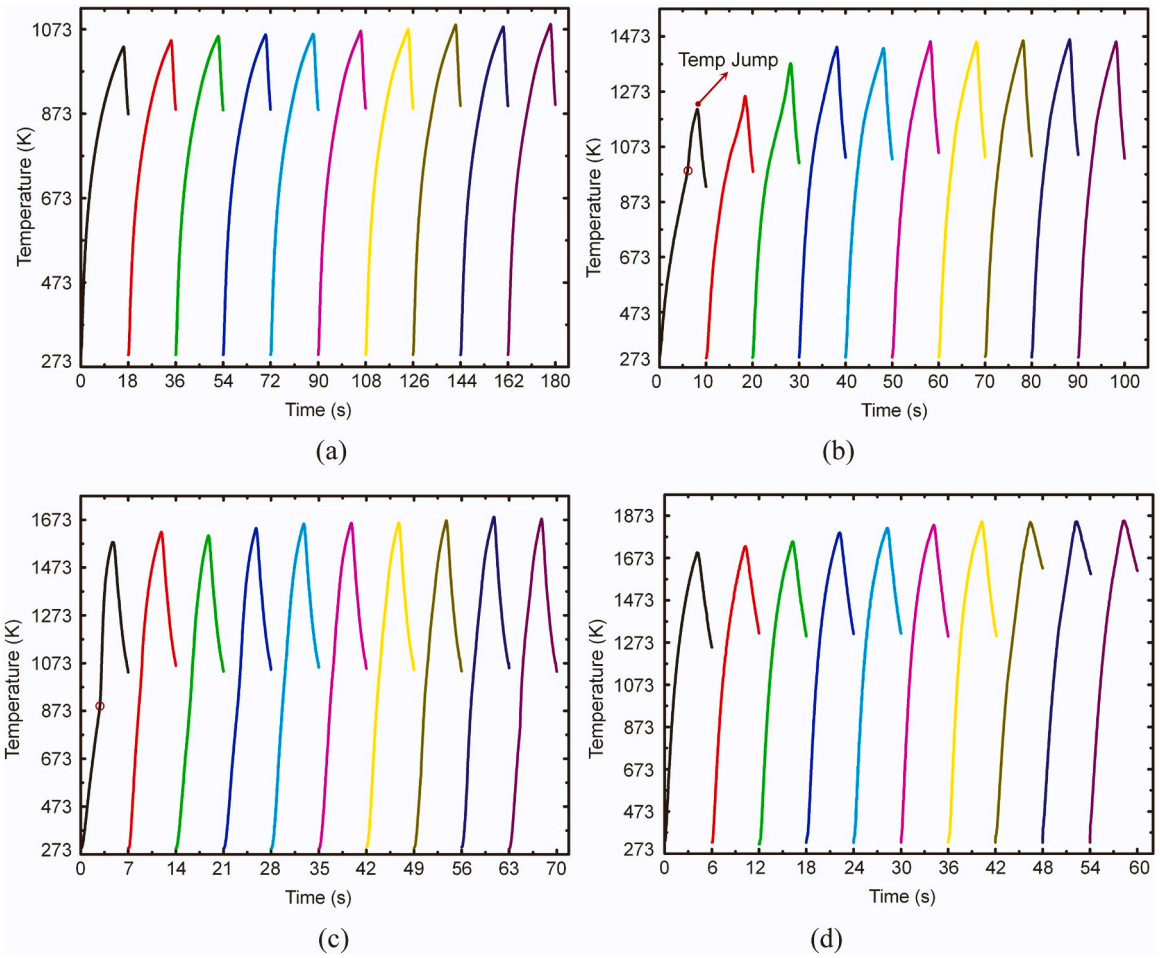

Fig. 8. The temperature curves of 2-D C/SiC-Ti_3SiC_2 composite at different laser power densities. (a) 318.3 W/cm^2; (b) 636.5 W/cm^2; (c) 954.8 W/cm^2; (d) 1273 W/cm^2.

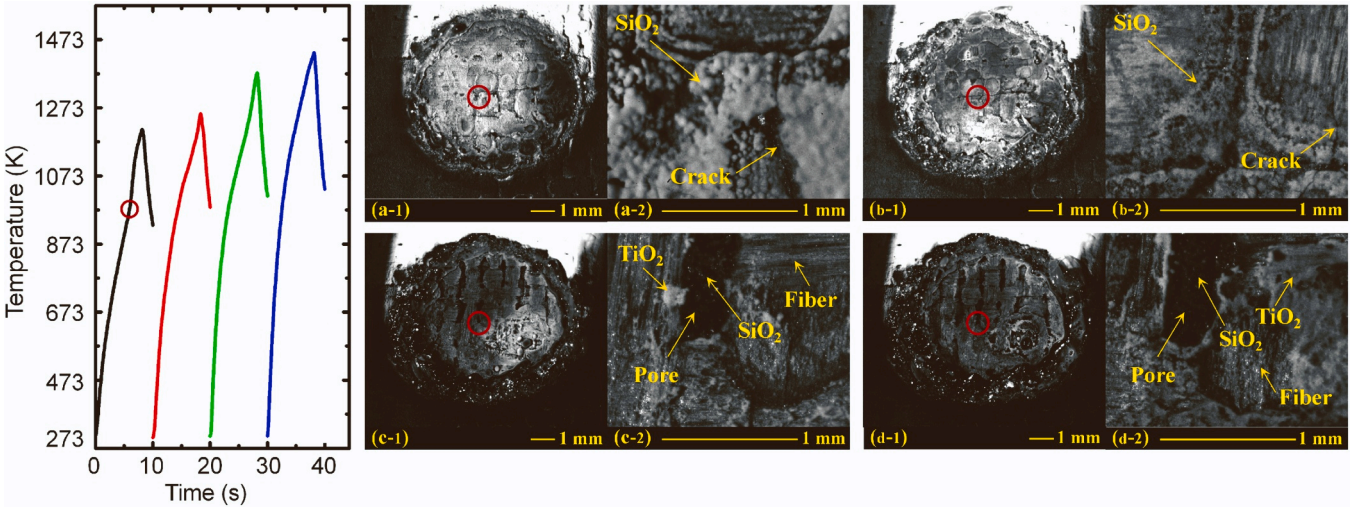

Fig. 9. Ablation morphology of "Temperature Jump" when the laser power density is 636.5 W/cm^2. (a) First irradiation; (b) second irradiation; (c) third irradiation; (d) fourth irradiation.

1273 W/cm^2, but the maximum temperature rises to more than 1732 K.

Fig. 10 shows the maximum temperature of the specimen after each laser irradiation under different LPDs. The linear fitting of the maximum temperature experimental data points is carried out. As shown in Fig. 10a and b, it is evident that the rule curve has three characteristics. The first feature is an obvious step point that occurs when LPD is 636.5 W/cm^2, which can also be summarized as a "Temperature Jump" phenomenon. The main reason of this phenomenon is the ablation of silicon carbide in the initial layer. The second characteristic is that the highest temperature is nearly linear with the laser irradiation times

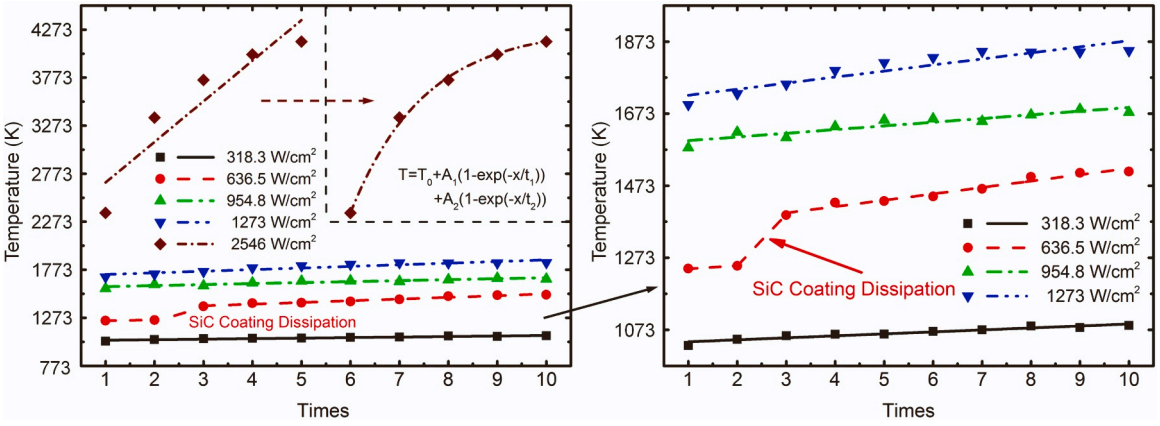

Fig. 10. The maximum temperature variation of 2-D C/SiC-Ti_3SiC_2 composite under different laser power densities.

under less than 1273 W/cm^2. The main reason is that the thickness of the specimen decreases due to the oxidizing reaction of silicon carbide and carbon fiber. Addedly, the overall linear slope also shows that the oxidation rate of carbon fiber increases with increasing LPD. The third characteristic is that the maximum temperature data no longer be consistent with the linear law but presents a nonlinear change when LPD increases to 2546 W/cm^2. The temperature obtained by the first laser irradiation is low, mainly because the first irradiation not only has the thermal protection effect of SiC coating, but also the initial thickness is thicker. So the temperature is much lower than that obtained by subsequent laser irradiation.

To summarize, the laser ablation resistance of 2-D C/SiC-Ti_3SiC_2 composite is related to LPD when the total output laser energy is constant. The initial SiC layer can effectively resist laser irradiation by its passive oxidation and Ti_3SiC_2 MAX phase-modified C/SiC composite is reusable when LPD is lower than 318.3 W/cm^2. This is an essential superiority of ultra-high temperature ceramics (UHTCs). Although the SiC matrix transforms from passive to active oxidation and loses the inhibition of carbon fiber oxidation, Ti_3SiC_2 MAX phase will be oxidized to form molten titanium dioxide, which can attach to the fiber and inhibit oxygen from contacting the carbon fiber at LPD is 636.5 W/cm^2. Furthermore, it still reduces the influence of heat affected zone on the overall performance of composite materials due to excellent high-temperature performance when LPD is between 636.5 and 1273 W/cm^2. When LPD increases to 2546 W/cm^2, the temperature of the laser irradiation surface promptly reaches over 3500 K. The heat released by the sublimation reaction of carbon fibers plays a prominent role in reducing ablation. Consequently, the performance of laser ablation resistance also depends on the carbon fiber content of the C/SiC composites. This is the main reason why the ablation resistance of 2-D C/SiC (the carbon fiber content is 54.2 %) is better than 3DN C/SiC (the carbon fibers content is 36.1 %) in Ref[36].

3.2.2. Mechanism of "Temperature jump"

In order to explain the mechanisms of "Temperature Jump" phenomena, the interface energy balance is established to discuss the influence of parameters in laser irradiation. The interface energy balance formula is shown below

$$q_{in} = -\kappa \nabla T\big|_w \cdot \hat{n} = \alpha q_{laser} - h_f(T_w - T_\infty) - \varepsilon\sigma\left(T_w^4 - T_\infty^4\right) + \dot{m}_w Q_w \quad (1)$$

Where$q_{in}$is the total input heat flux,$\kappa$is the thermal conductivity,$\nabla T|_w$is the temperature gradient at the interface,$\hat{n}$is the direction vector,$\alpha$is the laser absorptivity of the material,$q_{laser}$is the surface heat flux of laser,$h_f$is the coefficient of convective heat transfer,$T_w$is the interface temperature,$T_\infty$is the distant temperature,$\varepsilon$is the thermal radiation coefficient,$\sigma$is the Stephen Boltzmann constant,$\dot{m}_w$is the mass flow rate of the oxidation,$Q_w$is the reaction heat of oxidation.

As shown in Eq.1, there are two potential reasons of the suddenly increasingq_{in}. One is the discontinuity of laser absorptivity, and the other one is the change of oxidation exothermic heat flow caused by the mass flow rate of different oxidation. According to Ref [42], the laser absorptivity of the C/SiC composite is 0.86 at room temperature. It will change with the increase of surface temperature, 0.88, 0.90 and 0.89 at 1700, 1900 and 2100 K, respectively. Notwithstanding, the laser absorptivity of the C/SiC composite is variable but continuous. It's not the mechanism that causes the "Temperature Jump". For the oxidation behaviors of SiC, then$\dot{m}_w$is equal to multiply$B'$by$\rho_e u_e C_M$, where$B'$is non-dimensional mass flux,$\rho_e u_e C_M$is the bulk mass flux from the ambient to the surface. When the oxidation behavior is passive,$B'$is zero, so the oxidizing reaction does not affect the total input heat flux. When the passive transform to active oxidation,$B'$is equal to 0.3, and$\dot{m}_w Q_w$is approximately equivalent to 55 W/cm^2 [43].

Combined with the previous ablation morphology and temperature rise curve, there are two mechanisms of "Temperature Jump" for 2-D C/SiC and MAX phase-modified composites. The mechanism diagram of "Temperature Jump" is shown in Fig. 11. One is the conversion from passive oxidation of initial SiC coating to active oxidation [43,44], and the other is the conversion of SiC to fiber oxidation after complete dissipation of active oxidation. Therefore, when the oxidation changes at low laser power density, that is, from passive to active oxidation and from active oxidation of SiC to fiber oxidation, the oxidation heat release rate changes, the interface temperature gradient changes step by step, so the phenomenon of "Temperature Jump" will occur.

3.3. Evolution of ablation behavior with laser power density

3.3.1. Ablation rate

Fig. 12 gives the linear and mass ablation rates of 2-D C/SiC and 2-D C/SiC-Ti_3SiC_2 composites under different laser power densities. The liquid SiO_2 is produced due to the passive oxidation of SiC coating when LPD is 318.3 W/cm^2. The resultant effect is the transformation into a bubble-like solid SiO_2 after the termination of laser irradiation, adhering to the surface of the specimen. The expansion in volume and the introduction of oxygen contribute to both negative values in terms of linear and mass ablation rates. These data also underscore that the SiC demonstrates commendable oxidation resistance when the laser power density remains below 318.3 W/cm^2. However, as the laser power density surpasses 636.5 W/cm^2, discernible from the ablation data, the modified phase Ti_3SiC_2 effectively enhances the ablation resistance of C/SiC composites. As shown in Fig. 12a, the linear ablation rate reposefully increases. it is 1.13 μm/s, 3.96 μm/s and 9.51 μm/s, respectively, when LPD increases from 636.5 to 1273 W/cm^2. The specimen is burn-through when LPD is 2546 W/cm^2 and the linear ablation rate is not included. In comparison to 2-D C/SiC composites, the linear ablation

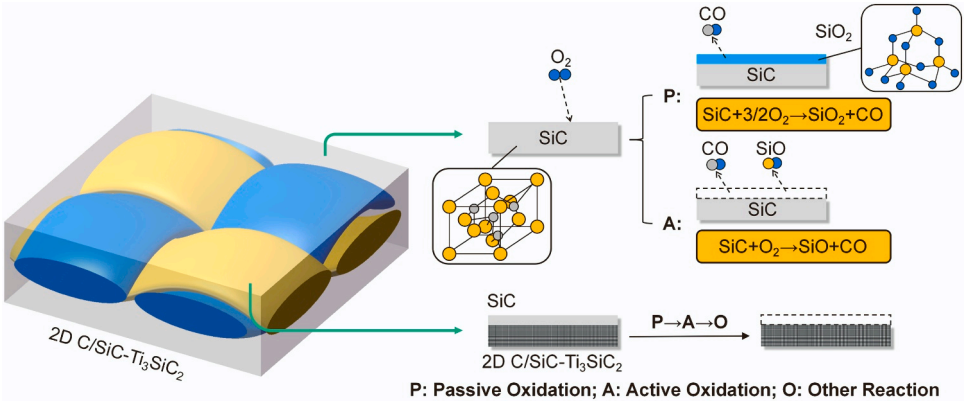

Fig. 11. Mechanism diagram of "Temperature Jump".

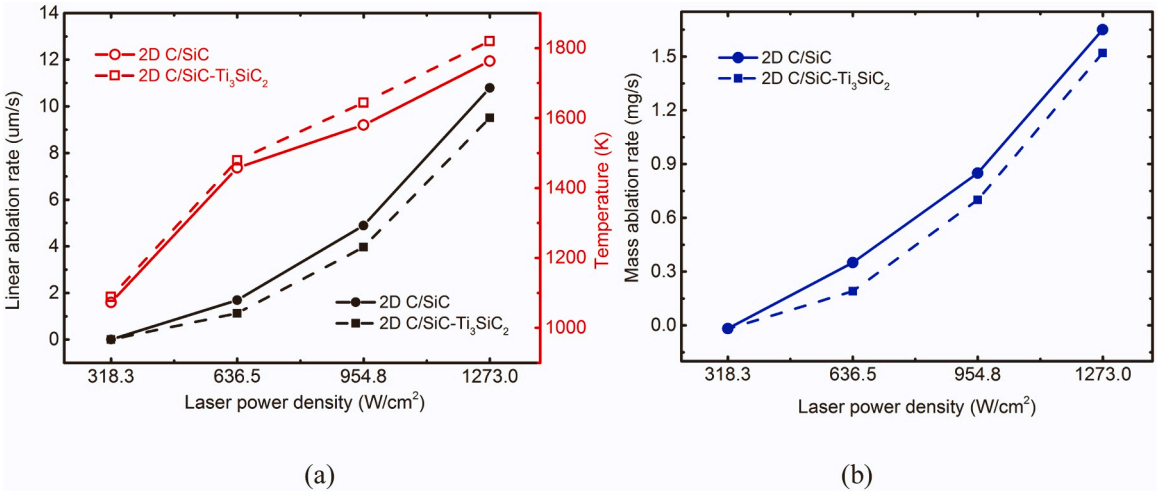

Fig. 12. The ablation data of 2-D C/SiC-Ti_3SiC_2.vs. 2-D C/SiC at different laser power densities. (a) Linear ablation rate; (b) mass ablation rate.

rate of 2-D C/SiC-Ti_3SiC_2, denoted as "L" and "L_{MAX}" for 2-D C/SiC and 2-D C/SiC-Ti_3SiC_2 respectively ($(L - L_{MAX})/L$as per the calculation formula), experiences reductions of 46.7 %, 19.0 %, and 11.9 %. The mass ablation rate, calculated similarly to the linear ablation rate formula, encounters decreases of 52.8 %, 18.4 %, and 8.0 %. Meanwhile, the temperature response depicted in Fig. 12a illustrates the efficacy of the Ti_3SiC_2 MAX ceramic phase in ameliorating the porosity of C/SiC composites, consequently elevating the thermal conductivity. Simultaneously, owing to the metallic attributes of Ti_3SiC_2, characterized by a notably elevated thermal conductivity, the in-plane and out-plane thermal conductivities of the modified composite exceed those of the 2-D C/SiC composite. Thus, the back surface temperature of the former surpasses that of the 2-D C/SiC composite.

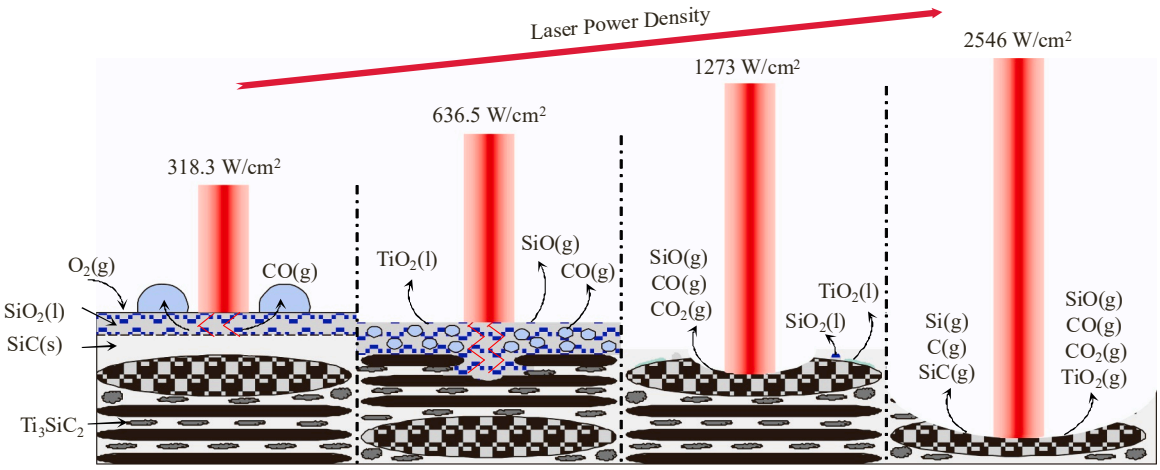

Fig. 13. Schematic diagram of ablation mechanism under different laser power densities.

3.3.2. Diagram of ablation mechanisms

According to the mesoscopic instantaneous ablation behaviors and the macro/meso/microscopic ablation morphology, Fig. 13 summarizes the schematic diagram of the main ablation mechanism under different laser power densities. Only the ablation characteristics of the Central Zone are concluded. The main reason is that the ablation behavior of CZ is more representative when LPD is 318.3–2546 W/cm^2. The ablation behavior of TZ is only a local phenomenon formed by the power density distribution and the temperature gradient. The white silica powder in EZ can be used to assist in the analysis of the leading chemical reactions in CZ, which does not occupy a dominant position in the analysis of the laser ablation mechanism. And the main chemical reactions are involved in formulas (2) to (15).

$$SiC(s) + 3/2\ O_2(g) \rightarrow SiO_2(l) + CO(g) \quad (2)$$

$$C(s) + 1/2\ O_2(g) \rightarrow CO(g) \quad (3)$$

$$C(s) + O_2(g) \rightarrow CO_2(g) \quad (4)$$

$$SiC(s) + O_2(g) \rightarrow SiO(g) + CO(g) \quad (5)$$

$$SiO(g) + 1/2\ O_2(g) \rightarrow SiO_2(s) \quad (6)$$

$$SiC(s) + 2SiO_2(l) \rightarrow 3SiO(g) + CO(g) \quad (7)$$

$$Ti_3SiC_2(s) + 5\ O_2(g) \rightarrow 3TiO_2(l) + SiO_2(l) + 2CO(g) \quad (8)$$

$$TiSi_2(s) + 3\ O_2(g) \rightarrow TiO_2(l) + 2SiO_2(l) \quad (9)$$

$$TiC(s) + 2\ O_2(g) \rightarrow TiO_2(l) + CO_2\ (g) \quad (10)$$

$$Ti_3SiC_2(s) \rightarrow 3TiC_x(s) + Si(l) \quad (11)$$

$$SiC\ (s) \rightarrow Si\ (l) + C\ (s) \quad (12)$$

$$2Si\ (g) + O_2(g) \rightarrow 2SiO(g) \quad (13)$$

$$SiC\ (s) \rightarrow SiC\ (g) \quad (14)$$

$$C\ (s) \rightarrow C\ (g) \quad (15)$$

It can be seen from Fig. 13 and formulas that the silicon carbide mainly undergoes passive oxidation (2), which produces a liquid SiO_2 film with a stable molecular structure when LPD is 318.3 W/cm^2. Nevertheless, the CO gas generated in the reaction process overflows outward. It acts on the inside of the film, making the liquid SiO_2 film becomes transparent bubbles with a diameter of a millimeter. When the laser with a power density of 636.5 W/cm^2 irradiates on 2-D C/SiC-Ti_3SiC_2 composite, it mainly occurs (2)-(10). The oxygen that reacts with the carbon fiber may come from the pores of the composite or diffuse into the interior of the composite through the SiO_2 thin layer from the air. Then the reaction of SiC coating and matrix transforms from passive oxidation to active oxidation, and the oxidation resistance is replaced by Ti_3SiC_2. When LPD increases to 1273 W/cm^2, the following reactions (2)-(13) occur, different from the ablation characteristics under 636.5 W/cm^2, the oxidation degree of carbon fiber is more serious. In the ablation process with a LPD of 2546 W/cm^2, the central area can be quickly heated to a very high temperature. According to the existence of a large number of ablated fibers in the central area and the fluffy carbon ash in the environment after the experiment, the temperature can be estimated, even up to 3500 K. At this temperature, SiC and Ti_3SiC_2 reach decomposition temperature (about 2800 K and 2570 K at ambient pressure) and sublimation temperature (about 3000 K), which produces mixed hot steam and gas escape. At this time, the carbon nanoparticles generated by the thermal decomposition of SiC are distributed in the gaps of the fiber, as shown in Fig. 5e. The above reactions of Ti_3SiC_2 also can absorb a lot of laser energy, so the MAX phase Ti_3SiC_2 can improve the ablation resistance of C/SiC composites. In the meantime, the carbon fiber also reaches the sublimation temperature and turns into carbon vapor, so reactions (2)-(15) may occur in the whole ablation process.

4. Conclusions

The present work experimentally illustrates the effect of laser power density on the ablation behaviors of 2-D C/SiC-Ti_3SiC_2 composite. The laser ablation mechanism is revealed from the instantaneous mesoscopic ablation behavior and the ablation morphology at macro/micro/micro scales. An in-situ observation measurement is established to obtain the real-time laser ablation behavior in meso-scale. Meanwhile, it can also conveniently shoot the irradiated morphology at the macro-scale and meso-scale, thus shortening the representation time. The microscopic morphology and micro-structure are obtained by scanning electron microscope (SEM) and X-ray energy dispersive spectroscopy (EDS) for determining the laser ablation mechanism. The temperature is measured by the platinum-rhodium thermocouple and infrared thermal imager, and the mechanism of "Temperature Jump" phenomenon is also discussed. The above experimental results give the laser ablation mechanisms of 2-D C/SiC-Ti_3SiC_2 composite under different laser power densities.

(1) The instantaneous process of formation, flowing and merging of SiO_2 bubbles, and fiber oxidation are obtained when the laser power density is 318.3 W/cm^2 and 636.5 W/cm^2, respectively. The microscopic morphology of the laser ablation central zone changes from SiO_2 bubbles to spherical SiO_2, from lamellate TiO_2 to smooth, and from spike-like carbon fibers to rough and finally irregular state carbon fibers with the increasing laser power density.
(2) "Temperature Jump" phenomena occur when the interface energy balance changes. Two conditions change the oxidation heat release rate. One is the conversion from passive oxidation of initial SiC coating to active oxidation. The other is the conversion of SiC to fiber oxidation after complete dissipation of active oxidation. Then the interface temperature gradient changes step by step, so the "Temperature Jump" phenomenon occurs.
(3) The laser ablation resistance of 2-D C/SiC-Ti_3SiC_2 composite is related to the laser power density. When the laser power density is 318.3 W/cm^2, the SiC coating is mainly passively oxidized to generate a dense and stable SiO_2 liquid layer, which inhibits the diffusion of oxygen into the material, thus improving ablation resistance. When the laser power density increases to 636.5 W/cm^2, the SiC coating and matrix oxidize actively and lose the anti-oxidation effect. However, the liquid TiO_2 generated by the oxidation of the Ti_3SiC_2 MAX phase adheres to the carbon fiber, thereby improving the oxidation resistance of the C/SiC composites. When the laser power density is 2546 W/cm^2, the temperature increase rapidly to 3500 K. In this condition, SiC and Ti_3SiC_2 mainly undergo decomposition and sublimation. Then the ablation resistance is related to the carbon content.

CRediT authorship contribution statement

Te Ma: Investigation Conducting, Experimental System Construction, Data Curation, Writing-Original Draft. **Hongwei Song**: Conceptualization, Supervision, Writing-Review & Editing, Project administration. **Cheng Qiu**: Investigation, Writing-Review & Editing. **Wu Yuan**: Investigation, Experimental Assistance. **Ruixing Wang**: Investigation, Mechanism analysis.

Declaration of Competing Interest

The authors declare that they have no known competing financial interests or personal relationships that could have appeared to influence the work reported in this paper.

Data availability

Data will be made available on request.

Acknowledgment

Financial supports from National Natural Science Foundation of China (Grant Nos. 11972035, 11972033, 12102434 and 12272379) are gratefully acknowledged. The authors would like to express their appreciation to Professor Laifei Cheng at the Science and Technology on Thermostructural Composite Materials Laboratory, Northwestern Polytechnical University, for providing the test specimens and analysis of ablation mechanisms.

Appendix A

The Archimedes drainage method is used to test the bulk density D_0 and open porosity P_0.

The calculation formulas are provided as follows:

$$P_0 = \frac{m_3 - m_1}{m_3 - m_2} \times 100\% \tag{A1}$$

$$D_0 = \frac{m_1 d}{m_3 - m_2} \times 100\% \tag{A2}$$

Where P_0 is the open porosity (vol%), D_0 is the bulk density (g/cm^3), d is the density of water (g/cm^3), m_1 is the mass of the dry sample (dry weight) (g), m_2 is the mass of saturated sample immersed in water (buoyant weight) (g), m_3 is the mass of impregnated saturated sample in air (wet weight) (g).

The experimental procedure is as follows: The specimen is placed in a 200 °C oven and dried for 2 h, then removed and cooled to room temperature. The dry weight (m_1) is measured. The specimen is suspended in an open container containing distilled water and placed in a vacuum system to reduce the pressure inside the container to below 2600 Pa. After maintaining this vacuum for 10 min, the specimen is slowly submerged in the distilled water until fully immersed. After an additional 30 min, the vacuum is released, and the container is allowed to stand in ambient air for 30 min. The buoyant weight (m_2) is measured. Subsequently, the specimen is removed, excess water droplets on the surface are gently wiped off using a damp cloth, and the wet weight (m_3) is measured.

Finally, leveraging the known volumetric fraction of carbon fibers, the content of SiC and Ti_3SiC_2 can be extrapolated based on the volumetric density and porosity of the composite.

Fig.A1 shows the laser ablation morphology of 2-D C/SiC composite at different scales. Fig.A.2 gives the comparison of the microscale laser ablation morphology of 2-D C/SiC and 2-D C/SiC-Ti_3SiC_2 composites.

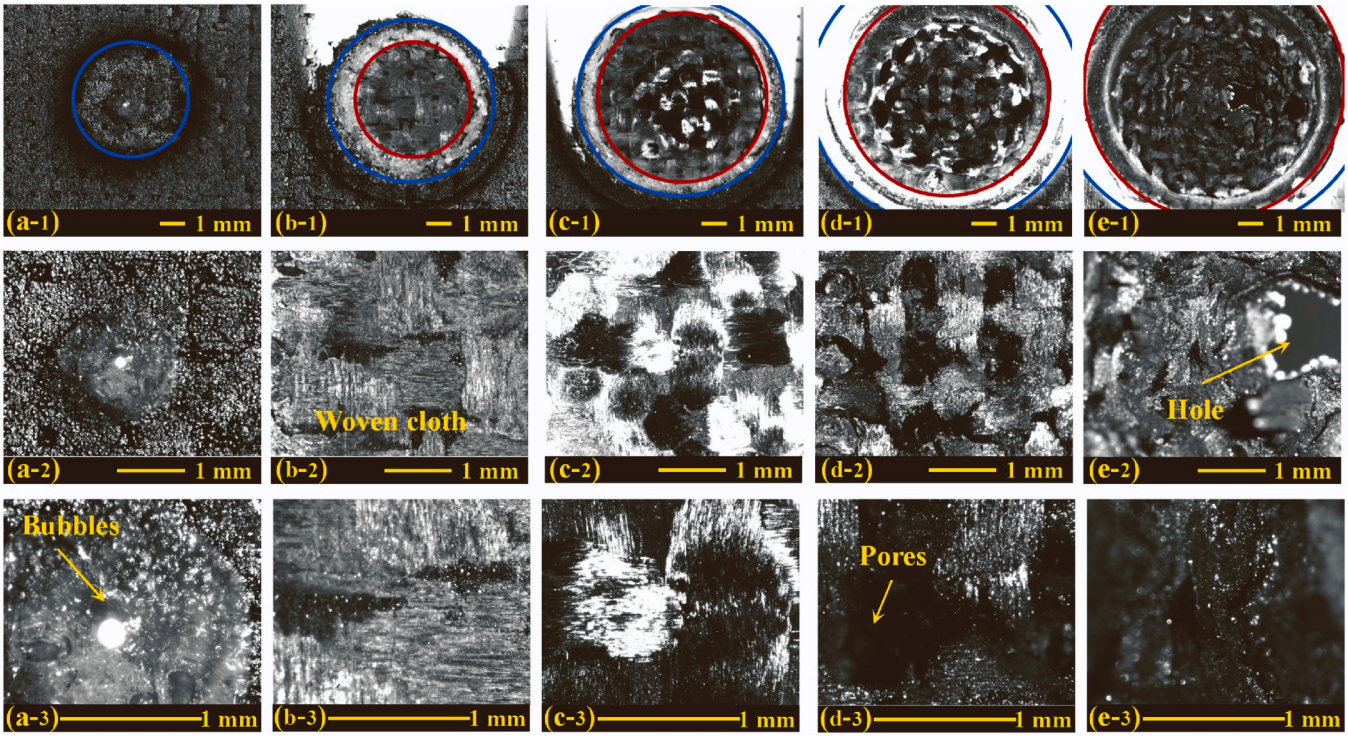

Fig. A1. The laser ablation morphology of 2-D C/SiC composite at different laser power densities. (a) 318.3 W/cm^2; (b) 636.5 W/cm^2; (c) 954.8 W/cm^2; (d) 1273 W/cm^2; (e) 2546 W/cm^2. 1, 2, and 3 represent the ablation morphology at macro-scale, after three times magnification and six times magnification, respectively.

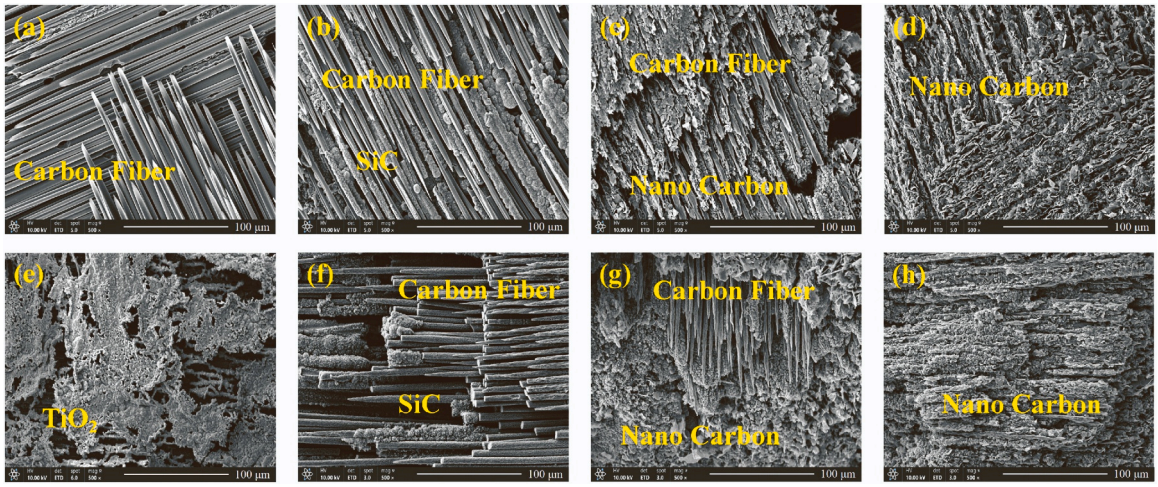

Fig. A2. The microscale laser ablation morphology of 2-D C/SiC composite at different laser power densities (a) 636.5 W/cm^2; (b) 954.8 W/cm^2; (c) 1273 W/cm^2; (d) 2546 W/cm^2. vs. 2-D C/SiC-Ti_3SiC_2 composite (e) 636.5 W/cm^2; (f) 954.8 W/cm^2; (g) 1273 W/cm^2; (h) 2546 W/cm^2.

.

References

[1] H. Bohrk, Transpiration Cooling at Hypersonic Flight-AKTiV on SHEFEX II. In: Proceedings of the 11th AIAA/ASME Joint Thermophysics and Heat Transfer Conference, Atlanta, GA, AIAA. (2014) 2014–2676. https://doi.org/10.2514/6.2014–2676.

[2] Q. Zhang, G. Li, A review of the application of C/SiC composite in thermal protection system, Multidiscip. Model. Mater. Struct. 5 (2009) 199–203, https://doi.org/10.1163/157361109787959903.

[3] J.H. Wang, L.J. Zhao, X.C. Wang, J. Ma, J. Lin, An experimental investigation on transpiration cooling of wedge shaped nose cone with liquid coolant, Int J. Heat. Mass Trans. 75 (2014) 442–449, https://doi.org/10.1016/j.ijheatmasstransfer.2014.03.076.

[4] Y.H. Zhang, Y.S. Liu, L.Y. Cao, X.T. Zheng, Y.J. Cao, J. Wang, Q. Zhang, Construction of continuous heat conductive channel, a double harvest strategy to enhance thermal conductance and bending strength of C/SiC composites, J. Mater. Sci. Technol. 105 (2022) 101–108, https://doi.org/10.1016/j.jmst.2021.06.063.

[5] C.L. Yan, Q. Li, Y.A. Shi, P. Luo, L.Y. Chen, L. Long, R.J. Liu, Ablation behavior of Cf/ZrC-SiC and Cf/SiC composites produced by precursor infiltration and pyrolysis combined with gaseous silicon infiltration, Corros. Sci. 209 (2022), 110717, https://doi.org/10.1016/j.corsci.2022.110717.

[6] C. Zhang, T.H. Guan, T.F. Ren, X.Y. Zhang, B. Wang, X. Zhou, T. Suo, Influences of SiC infiltration and coating on compressive mechanical behaviours of 2-D C/SiC composites up to 1600°C at wide-ranging strain rates, J. Eur. Ceram. Soc. 42 (2022) 3787–3801, https://doi.org/10.1016/j.jeurceramsoc.2022.02.042.

[7] Y.Y. Huo, Q. Yang, S. Chen, S.H. Meng, J.Y. Zhao, J.Y. Jiang, Modeling and experimental study on electrical impedance response to damage accumulation in 2-D C/SiC composites, J. Eur. Ceram. Soc. 42 (2022) 4144–4153, https://doi.org/10.1016/j.jeurceramsoc.2022.04.001.

[8] L.B. Li, P. Reynaud, G. Fantozzi, Time-dependent creep fatigue damage evolution in C/SiC composite: theory and analytical prediction, Ceram. Int. 48 (2022) 20731–20742, https://doi.org/10.1016/j.ceramint.2022.04.054.

[9] Y.L. Tang, M.K. Yue, J.S. Zhang, Y. Li, X.F. Fang, X. Feng, Revealing thermal ablation mechanisms of C/SiC with in situ optical observation and numerical simulation, J. Eur. Ceram. Soc. 40 (2020) 3897–3905, https://doi.org/10.1016/j.jeurceramsoc.2020.04.010.

[10] Q. Zhang, J.R. Ge, B.B. Zhang, C.W. He, Z.Q. Wu, J. Liang, Effect of thermal residual stress on the tensile properties and damage process of C/SiC composites at high temperatures, Ceram. Int. 48 (2022) 3109–3124, https://doi.org/10.1016/j.ceramint.2021.10.085.

[11] Y.Z. Ma, X.W. Yin, X.M. Fan, P.F. Ju, X.L. Dang, Modification and toughening of 3D needled C/SiC composite by deformable MAX phase-based matrix, Mater. Sci. Eng. A 712 (2018) 397–405, https://doi.org/10.1016/j.msea.2017.11.110.

[12] O. Yaghobizadeh, A. Sedghi, H.R. Baharvandi, Mechanical properties and microstructure of the C-C-SiC, C-C-SiC-Ti_3SiC_2 and C-C-SiC-$Ti_3Si(Al)C_2$ composites, Mater. Sci. Eng. A 731 (2018) 446–453, https://doi.org/10.1016/j.msea.2018.06.069.

[13] O. Yaghobizadeh, A. Sedghi, H.R. Baharvandi, Effects of ZrC content on the synthesis of MAX phase and mechanical properties of C_f-C-SiC-Ti_3SiC_2-ZrC composites, Ceram. Int. 44 (2018) 18039–18047, https://doi.org/10.1016/j.ceramint.2018.07.006.

[14] G.M. Song, S.B. Li, C.X. Zhao, W.G. Sloof, S. van der Zwaag, Y.T. Pei, J.Th.M. De Hosson, Ultra-high temperature ablation behavior of Ti_2AlC ceramics under an oxyacetylene flame, J. Eur. Ceram. Soc. 31 (2011) 855–862, https://doi.org/10.1016/j.jeurceramsoc.2010.11.035.

[15] X.M. Fan, X.W. Yin, Microstructure and properties of carbon fiber reinforced SiC matrix composites containing Ti_3SiC_2, Adv. Eng. Mater. 16 (2014) 670–683, https://doi.org/10.1002/adem.201400081.

[16] X.M. Fan, X.W. Yin, Y.Z. Ma, L.T. Zhang, L.F. Cheng, Oxidation behavior of C/SiC-Ti_3SiC_2 at 800-1300 ℃ in air, J. Eur. Ceram. Soc. 36 (2016) 2427–2433, https://doi.org/10.1016/j.jeurceramsoc.2016.03.029.

[17] O. Yaghobizadeh, A. Sedghi, H.R. Baharvandi, Effect of Ti_3SiC_2 on the ablation behavior and mechanism of C_f-C-SiC-Ti_3SiC_2 composites under oxyacetylene torch at 3000 °C, Ceram. Int. 45 (2019) 777–785, https://doi.org/10.1016/j.ceramint.2018.09.244.

[18] X.T. Shen, K.Z. Li, H.J. Li, Q.G. Fu, S.P. Li, F. Deng, The effect of zirconium carbide on ablation of carbon/carbon composites under an oxyacetylene flame, Corros. Sci. 53 (2011) 105–112, https://doi.org/10.1016/j.corsci.2010.09.028.

[19] Y. Sui, M.H. Yuan, Z.N. Bai, Z.W. Fan, Recent development of high-energy short-pulse lasers with cryogenically cooled Yb:YAG, Appl. Sci. 12 (2022) 3711, https://doi.org/10.3390/app12083711.

[20] U. Brauch, C. Röcker, T. Graf, M.A. Ahmed, High-power, high-brightness solid-state laser architectures and their characteristics, Appl. Phys. B. 128 (2022) 58, https://doi.org/10.1007/s00340-021-07736-0.

[21] M.Q. Sun, X.D. Wang, S.M. Yang, J.Y. Pan, X. Geng, K.X. Li, M.X. Lu, S.G. Miao, S. W. Li, High-energy quasi-trapezoid noise-like pulse generation and harmonic operation in a fiber laser, Optik 259 (2022), 169038, https://doi.org/10.1016/j.ijleo.2022.169038.

[22] S. Liu, Z.J. Tian, L.D. Shen, M.B. Qiu, D.Q. Xie, G.D. Ma, Y.Y. Xu, H.F. Guo, Laser damage resistance of plasma-sprayed alumina and honeycomb skeleton/alumina composite ceramic coatings, Ceram. Int. 48 (2022) 7885–7896, https://doi.org/10.1016/j.ceramint.2021.11.336.

[23] A. Grabowski, A. Lisiecki, M. Dyzia, J. Labaj, S. Stano, The effect of laser wavelength on surface layer melting of the AlSi/SiC composite, J. Manuf. Process 75 (2022) 627–636, https://doi.org/10.1016/j.jmapro.2022.01.031.

[24] H.H. Wang, J.A. Kong, M. Xu, P.F. Zhang, L. Yang, X.H. Shi, H.J. Li, Laser ablation behavior of SiO_2-Nd_2O_3/Si-SiC-$MoSi_2$ coated C/C composites repaired by laser cladding, Corros. Sci. 198 (2022), 110132, https://doi.org/10.1016/j.corsci.2022.110132.

[25] X. Chen, J. Yin, X.J. Liu, B.B. Pei, J. Huang, X.L. Peng, A.D. Xia, L.Z. Huang, Z. R. Huang, Effect of laser power on mechanical properties of SiC composites rapidly fabricated by selective laser sintering and direct liquid silicon infiltration, Ceram. Int. 48 (2022) 19123–19131, https://doi.org/10.1016/j.ceramint.2022.03.203.

[26] M.M. Yang, T. Wang, M. Wu, Ablation behavior of SiC whisker and ZrB_2 particle-filled ZrO_2 sol-gel composite coating under high-intensity continuous laser irradiation, Ceram. Int. 47 (2021) 26327–26334, https://doi.org/10.1016/j.ceramint.2021.06.043.

[27] X. Li, W. Hou, B. Han, L.F. Xu, Z.W. Li, P.Y. Nan, X.W. Ni, Thermal response during volumetric ablation of carbon fiber composites under a high intensity continuous laser irradiation, Surf. Interfaces 23 (2021), 101032, https://doi.org/10.1016/j.surfin.2021.101032.

[28] M.J. Li, L.M. Chen, X.J. Yang, A feasibility study on high-power fiber laser cutting of thick CFRP laminates using single-pass strategy, Opt. Laser Technol. 138 (2021), 106889, https://doi.org/10.1016/j.optlastec.2020.106889.

[29] P.F. Shen, Y.P. Zhuang, S.D. Jiang, C.Y. Luo, X.P. Tong, Y.Y. Liang, Y. Yan, N. H. Zhang, L.Y. Zhang, Experimental and numerical investigation on the ablation mechanism of Al_2O_3/Al_2O_3-CMCs under continuous-wave laser irradiation, J. Eur. Ceram. Soc. 42 (2022) 2307–2318, https://doi.org/10.1016/j.jeurceramsoc.2022.01.005.

[30] W.N. Zhao, T. Ma, H.W. Song, W. Yuan, R.X. Wang, Z. Wang, L.L. Lu, C.G. Huang, Effects of tangential supersonic airflow on the laser ablation of laminated CFRP, J. Mater. Res. Technol. 14 (2021) 1985–1997, https://doi.org/10.1016/j.jmrt.2021.07.101.
[31] V. Allheily, F. Lacroix, A. Eichhorn, L. Merlat, G. L'Hostis, B. Durand, An experimental method to assess the thermo-mechanical damage of CFRP subjected to a highly energetic 1.07 mu m-wavelength laser irradiation, Compos Part B-Eng. 92 (2016) 326–331, https://doi.org/10.1016/j.compositesb.2016.02.024.
[32] Y.G. Tong, S.X. Bai, H. Zhang, Y.C. Ye, Laser ablation behavior and mechanism of C/SiC composite, Ceram. Int. 39 (2013) 6813–6820, https://doi.org/10.1016/j.ceramint.2013.02.012.
[33] Y.G. Tong, S.X. Bai, Y.L. Hu, X.B. Liang, Y.C. Ye, Q.H. Qin, Laser ablation resistance and mechanism of Si-Zr alloyed melt infiltrated C/C-SiC composite, Ceram. Int. 44 (2018) 3692–3698, https://doi.org/10.1016/j.ceramint.2017.11.141.
[34] J.T. Wang, Y.Z. Ma, Y.W. Liu, W. Yuan, H.W. Song, C.G. Huang, X.W. Yin, Experimental investigation on laser ablation of C/SiC composites subjected to supersonic airflow, Opt. Laser Technol. 113 (2019) 399–406, https://doi.org/10.1016/j.optlastec.2019.01.019.
[35] S.N. Pan, Q.Y. Li, Z.K. Xian, N.G. Su, F.Z. Zeng, The effects of laser parameters and the ablation mechanism in laser ablation of C/SiC composite, Materials 12 (2019) 3076, https://doi.org/10.3390/ma12193076.
[36] Z. Wang, J.T. Wang, H.W. Song, W. Yuan, Y.W. Liu, T. Ma, C.G. Huang, Laser ablation behavior of C/SiC composites subjected to transverse hypersonic airflow, Corros. Sci. 183 (2021), 109345, https://doi.org/10.1016/j.corsci.2021.109345.
[37] Z. Wang, R.X. Wang, H.W. Song, T. Ma, J.T. Wang, W. Yuan, C.G. Huang, Decoupling mechanisms of "avalanche" phenomenon for laser ablation of C/SiC composites in hypersonic airflow environment, Int J. Therm. Sci. 173 (2022), 107414, https://doi.org/10.1016/j.ijthermalsci.2021.107414.
[38] J. Lachaud, N. Bertrand, G.L. Vignoles, G. Bourget, F. Rebillat, P. Weisbecker, A theoretical/experimental approach to the intrinsic oxidation reactivities of C/C composites and of their components, Carbon 45 (2007) 2768–2776, https://doi.org/10.1016/j.carbon.2007.09.034.
[39] R. Raj, K. Terauds, Bubble nucleation during oxidation of SiC, J. Am. Ceram. Soc. 98 (2015) 2579–2586, https://doi.org/10.1111/jace.13613.
[40] C. Li, Y.R. Niu, T. Liu, X. Zhong, X.H. Pan, Y. Zeng, X.B. Zheng, C.X. Ding, Bubble phenomenon of ZrB2 based composites at high temperatures, Ceram. Int. 45 (2019) 6648–6654, https://doi.org/10.1016/j.ceramint.2018.12.153.
[41] S. Gangireddy, S.N. Karlsdottir, S.J. Norton, J.C. Tucker, J.W. Halloran, In situ microscopy observation of liquid flow, zirconia growth, and CO bubble formation during high temperature oxidation of zirconium diboride-silicon carbide, J. Eur. Ceram. Soc. 30 (2010) 2365–2374, https://doi.org/10.1016/j.jeurceramsoc.2010.01.034.
[42] Z. Zhang, M.F. Modest, Temperature-dependent absorptances of ceramics for Nd: YAG and CO_2 laser processing applications, J. Heat. Transf. 120 (1998) 322–327, https://doi.org/10.2351/1.5059039.
[43] S.Y. Chen, I.D. Boyd, Analysis of the silicon carbide boundary layer under passive and active oxidation, AIAA (2019) 17–21.
[44] N. Jacobson, B. Harder, D. Myers, Oxidation transitions for SiC Part I. Active-to-passive transitions, J. Am. Ceram. Soc. 96 (2013) 838–844, https://doi.org/10.1111/jace.12108.